

Angular momentum transport during X-ray bursts on neutron stars: a numerical general relativistic hydrodynamical study

A. Hujeirat¹ and F.-K. Thielemann²

¹ ZAH, Landessternwarte Heidelberg-Königstuhl,
Universität Heidelberg, 69120 Heidelberg, Germany

² Departement Physik, Universität Basel, Switzerland

Received ... / Accepted ...

ABSTRACT

Aims. The distribution of angular momentum of the matter during X-ray bursts on neutron stars is studied by means of 3D axisymmetric general relativistic hydrodynamics.

Methods. The set of fully general relativistic Navier-Stokes equations is solved implicitly using the implicit solver GR-I-RMHD in combination with a third order spatial and second order temporal advection scheme. The viscous operators are formulated using a Kerr-like metric in the fixed background of a slowly rotating neutron star whose radius coincides with the corresponding last stable orbit. The importance of these operators and their possible simplifications are discussed as well. To verify the consistency and accuracy of the solution procedure, the time-dependent evolutions of non-rotating heat bubbles during their rise to the surface of a white dwarf are followed and compared with previous calculations.

Results. In the rotating case and depending on the viscosity parameter, α_{tur} , it is found that the viscously-initiated fronts at the center of bursts propagate at much faster speed than the fluid motion. These fast fronts act to decouple angular momentum from matter: angular momentum is transported outwards while matter sinks inwards into the deep gravitational well of the neutron star, thereby enhancing the compression of matter necessary for initiating ignition, that subsequently spreads over the whole surface of the neutron star on the viscous time scale. Based on the numerical simulations, we find that a viscosity parameter $\alpha_{\text{tur}} = O(0.1)$ is most suitable for fitting observations of neutron stars during X-ray bursts. It is argued that the spin up observed in the cooling tails of X-ray bursts is a transient phase, which eventually should be followed by a spin down phase. This delay can be attributed to a significant lengthening of the viscous time scale due to rapid cooling of matter in the outer layers.

Conclusions.

Key words. General relativity: neutron stars – black holes – X-ray bursts, Methods: numerical – hydrodynamics – relativistic

Received ... / Accepted ...

1. Introduction

Part of the observed neutron stars (NSs) belong to the family of ultra-compact objects, in which general relativistic effects are prominent (Shapiro & Teukolsky, 1983; Stergioulas, 2003; Psaltis, 2008). Depending on the equation of state, NSs may live even inside their last stable orbits, making the conversion efficiency of gravitational energy into radiation even larger than that of accreting Schwarzschild black holes (BHs, Camenzind, 2007). In low mass X-ray binaries, relativistic jets have been also observed to emanate from around accreting NSs with bulk Lorentz factors that are comparable to those emanating from around black holes (Migliari, 2006, 2008).

On the simulation site, numerous general relativistic hydrodynamical calculations have been carried out to study different aspects of NSs, such as formation, merger, inner structure, accretion or jets around NSs (Thielemann, 1990; Liebendörfer et al., 2002; Marti & Müller, 2003; Özel & Psaltis, 2003; Shibata, 2003; McKinney, 2006; Shibata et al., 2006; Abdikamalov et al., 2008; Zachariah et al., 2008, see also the references therein)

Duez et al. (2004) carried out general relativistic calculations to study the formation of hypermassive NSs, taking into account the effect of viscosity. The authors found that viscosity drives the NS's inner core into rigid rotation and simultaneously transports angular momentum outwards into the outer envelope. As a consequence, the core is found to contract in a quasi-stationary manner while the outer layers expand to form a differentially rotating torus.

This behavior is similar to accretion of matter via rotating disks. Here the viscosity acts to decouple matter from angular momentum, in that it transports angular momentum outwards, while forcing the matter to sink deeper into the gravitational well of the central object (Pringle, 1981). In the absence of viscosity, angular momentum as well as magnetic fields in ideal MHD are frozen-in to the matter. Thus, while strong magnetic fields are essential to enable rigid rotation, viscosity, on the other hand, drives the outer layers into differential rotation.

The type of rotation in the outer layers, differential or rigid rotation, may have profound effects on the conditions leading to the X-ray bursts observed on NSs (Bildsten & Strohmayer, 1999; Spitkovsky et al., 2002).

Indeed, recent observations of X-ray bursts revealed the so called burst oscillations, in which a spin-up or spin-down of the NSs in their cooling tails have been detected, reaching a plateau on the asymptotic limit (see Strohmayer et al., 1997; Strohmayer & Markwardt, 1999; Strohmayer, 2001, for a de-

tailed discussion). It has been argued that the increase/decrease of the spin of NSs during bursts is connected to the redistribution of angular momentum of the thermonuclear shell (Strohmayer, 2001b). Accordingly, when a thermonuclear shell starts to expand at the burst onset, the moment of inertia increases while its spin decreases. When the shell starts to contract and subsequently recouples to the NS, the inertia decreases and the spin increases.

Also, several X-ray bursts on NSs display a spin down rather than spin up in their cooling tails (Strohmayer, 1999c). In this case, however, it was suggested that the spin down probably begins anew episode of thermonuclear energy release, most likely in layers underlying those responsible for the initial runaway. Cumming & Bildsten (2003), however, investigated in detail the hydrostatic expansion during bursts and the expected change of spin due to angular momentum conservation and concluded, that a shell expansion/contraction alone cannot explain the mechanisms underlying the observed spin-up/down of the NSs during bursts. Noteworthy is that the model in which ignition starts at a point and spreads over the whole surface of the NS via burning fronts appears to fit observations, which reveals that the X-ray emitting area increases during the bursts (Strohmayer et al., 1997). However, the role of rotation, the nature of these burning fronts and the manner they affect their surrounding are poorly understood.

In this paper we present a first attempt to model the rotational evolution of thermally induced bursts beneath the atmosphere of a rotating NS and to study the role and effects of the viscosity on the redistribution of angular momentum under strong gravitational field conditions. Our investigation relies on employing a general relativistic hydrodynamical solver, in which turbulent-eddies have the effect of friction that gives rise to an enhanced re-distribution of angular momentum.

The paper runs as follows: In Section 2 we describe the additional viscous operators that have been incorporated into the solver to study the viscous-redistribution of angular momentum. The results of several model calculations aimed at studying the distribution of angular momentum during X-ray bursts on NSs are presented and discussed in Section 3, while in Sec. 4 the results are summarized.

2. The general relativistic Navier-Stokes equations

The set of the general relativistic hydrodynamical equations and their derivations are well described in Sec. 2 of Hujeirat et al. (2008). In this section we list the viscous operators of the momentum equations, which we have incorporated into the implicit solver.

The stress energy tensor for viscous flows has the following form (Richardson & Chung, 2002; Font, 2003; Camenzind, 2007):

$$T^{\mu\nu} = T_{\text{PF}}^{\mu\nu} + \left\{ T_{\text{Vis}}^{\mu\nu} \right\} = \rho h u^\mu u^\nu + P g^{\mu\nu} + \left\{ -\eta[\bar{\sigma}^{\mu\nu} + \frac{\Theta}{3} h^{\mu\nu}] \right\}, \quad (1)$$

where μ, ν are indices that correspond to the four coordinates $\{t, r, \theta, \varphi\}$ and $T_{\text{PF}}^{\mu\nu}$, $T_{\text{Vis}}^{\mu\nu}$ denote the stress energy tensor due to perfect and viscous flows, respectively. P , η , Θ , are the pressure, which is calculated from the equation of state corresponding to a polytropic or to an ideal gas, the dynamical viscosity which is assumed to be identical to the shear viscosity, and Θ ($\equiv \nabla_\mu u^\mu$), which measures the divergence or convergence of the fluid world lines, respectively. $h^{\mu\nu} = u^\mu u^\nu + g^{\mu\nu}$ is the spatial projection tensor, whereas $\bar{\sigma}$ corresponds to the symmetric spatial shear tensor: $\bar{\sigma}^{\mu\nu} = \nabla_\zeta u^\mu h^{\nu\zeta} + \nabla_\zeta u^\nu h^{\mu\zeta}$.

For the X-ray burst calculations, the general relativistic Navier-Stokes equations are solved using the Boyer-Lindquist coordinates in the background of a slowly rotating NS, with the following metric elements:

$$g_{\mu\nu} = \begin{pmatrix} g_{tt} & 0 & 0 & g_{t\varphi} \\ 0 & g_{rr} & 0 & 0 \\ 0 & 0 & g_{\theta\theta} & 0 \\ g_{\varphi t} & 0 & 0 & g_{\varphi\varphi} \end{pmatrix},$$

where

$$\begin{cases} g_{tt} &= \beta_\varphi \beta^\varphi - \alpha^2 \\ g_{t\varphi} &= g_{\varphi t} = \beta_\varphi = g_{\varphi\varphi} \beta^\varphi \\ g_{rr} &= \frac{\bar{\rho}^2}{\Delta}, \quad g_{\theta\theta} = \bar{\rho}^2, \quad g_{\varphi\varphi} = \bar{\omega}^2 \\ \Delta &= r^2 - 2r_g r + \Omega_{\text{NS}}^2 \\ \bar{\rho}^2 &= r^2 + \Omega_{\text{NS}}^2 \sin^2 \theta \\ \Sigma^2 &= (r^2 + \Omega_{\text{NS}}^2)^2 - \Omega_{\text{NS}}^2 \Delta \cos^2 \theta \\ \bar{\omega} &= \frac{\Sigma}{\bar{\rho}} \cos \theta \\ \alpha^2 &= \frac{\rho^2}{\Sigma^2} \Delta \\ \beta^r &= \beta^\theta = 0 \\ \Upsilon &= \frac{\bar{\rho}^2 \Sigma^2}{\Delta} \cos^2 \theta \\ \sqrt{-g} &= \bar{\rho}^2 \cos \theta = \alpha \sqrt{\Upsilon}. \end{cases} \quad (2)$$

In this formulation, the parameter “ Ω_{NS} ” denotes the spin of the neutron star, which is taken to be much smaller than the break-up frequency. β^φ is the frame-dragging frequency associated with the rotation of the NS:

$$\beta^\varphi = \Omega_{\text{FD}} = \left[\frac{2G}{c^2} \right] J_* \left(\frac{r}{\Sigma^2} \right) = \left[\frac{2GM}{c^2} \right] \left(\frac{1}{r^3} \right) R_{\text{NS}}^2 \Omega_{\text{NS}}, \quad (3)$$

where $J_* = I_* \Omega_{\text{NS}}$, and $I_* = \frac{2}{5} M_{\text{NS}} R_{\text{NS}}^2$ is the moment of inertia of the NS. The parameters: c , M_{NS} , G , $r_g (= \frac{GM_{\text{NS}}}{c^2})$, α denote the speed of light, mass of the NS, the gravitational constant, the gravitational radius and the lapse function, respectively. In writing these expressions, we made use of the coordinate transformation $\bar{\theta} = \pi/2 - \theta$, where we use the latitude θ instead of the polar distance angle $\bar{\theta}$; hence the appearance of “cos” instead of “sin” in the metric terms.

The set of general relativistic Navier-Stokes equations in 3D axisymmetry can be written as the residual vector equation:

$$\mathbf{R} = 0. \quad (4)$$

The components of this vector read as follows:

1. The continuity equation

$$R_1 = \frac{\partial D}{\partial t} + L_{1r\theta} D = 0 \quad (5)$$

2. The radial momentum equation

$$R_2 = \frac{\partial M_r}{\partial t} + L_{1r\theta} M_r - f_r - L_{2r\theta}^r M_r = 0 \quad (6)$$

3. The vertical momentum equation

$$R_3 = \frac{\partial M_\theta}{\partial t} + L_{1r\theta} M_\theta - f_\theta - L_{2r\theta}^\theta M_\theta = 0 \quad (7)$$

4. The angular momentum equation

$$R_4 = \frac{\partial M_\varphi}{\partial t} + L_{1r\theta} M_\varphi - f_\varphi - L_{2r\theta}^\varphi M_\varphi = 0 \quad (8)$$

5. The internal energy equation

$$R_5 = \frac{\partial \mathcal{E}^d}{\partial t} + L1_{r\theta} \mathcal{E}^d + (\gamma - 1) \mathcal{E}^d \left[\frac{\partial u^t}{\partial t} + L1_{r\theta} u^t \right] = 0, \quad (9)$$

where $L1_{r\theta}$ are first order advection operators that have the form:

$$\begin{aligned} L1_{r\theta} q &= \frac{1}{\sqrt{-g}} \frac{\partial}{\partial r} (\sqrt{-g} q V^r) + \frac{1}{\sqrt{-g}} \frac{\partial}{\partial \theta} (\sqrt{-g} q V^\theta) \\ &= \bar{\nabla}_r \cdot q V^r + \bar{\nabla}_\theta \cdot q V^\theta. \end{aligned}$$

$f_{r,\theta,\varphi}$ are force terms that include pressure gradients, centrifugal and gravitational forces acting along the radial, horizontal and azimuthal directions, respectively. $D(\doteq \rho u^t)$ is the modified relativistic mass density. M_μ are the four-momenta: $(M_t, M_r, M_\theta, M_\varphi) \doteq \bar{D}(u_t, u_r, u_\theta, u_\varphi)$, where $\bar{D} \doteq Dh$, and u^t is the time-like velocity, $V^\mu = u^\mu / u^t$ is the transport velocity and ‘‘h’’ denotes the enthalpy. $L2_{r\theta}^\xi$ are the spatial projections of the viscous stress energy tensor $T_{\text{Vis}}^{\mu\nu}$ (see Eq. 1) in the respective direction. These are obtained from the projection of the viscous tensor along the vector normal to the hyperspace, i.e., constant in time:

$$L2_{r\theta}^\xi = \nabla_\mu T_{\text{Vis}}^{\mu\xi} = \bar{\partial}_\mu T_{\text{Vis}}^{\mu\xi} + \Gamma_{\mu\lambda}^\xi T_{\text{Vis}}^{\mu\lambda},$$

where $\xi = \{r, \theta, \varphi\}$. ∇_μ corresponds to the spatial divergence of a tensor taken in the Boyer-Lindquist coordinates and $\Gamma_{\mu\lambda}^\xi$ are the Christoffel’s symbols of the second kind.

For completeness, we re-write the forms of these second order viscous operators explicitly as follows:

$$\begin{aligned} L2_{r\theta}^r &= \bar{\nabla}_r \cdot \eta \left[\left(\frac{\partial u^r}{\partial r} + \frac{1}{2} (g^{rr} \frac{\partial g_{rr}}{\partial r}) u^r \right) (u_r u^r + 1) \right. \\ &\quad \left. + \frac{\partial u_r}{\partial r} - \frac{1}{2} (g^{rr} \frac{\partial g_{rr}}{\partial r}) u^r \right] ((u^r)^2 + g^{rr}) \\ &\quad - \frac{2}{3} (\bar{\nabla}_r \cdot u^r + \bar{\nabla}_\theta \cdot u^\theta) (u_r u^r + 1) \\ &\quad + \bar{\nabla}_\theta \cdot \eta \left[\left(\frac{\partial u^\theta}{\partial r} + \frac{1}{2} (g^{\theta\theta} \frac{\partial g_{\theta\theta}}{\partial r}) u^\theta \right) (u_r u^r + 1) \right. \\ &\quad \left. + \frac{\partial u_r}{\partial \theta} + \frac{1}{2} (g^{\theta\theta} \frac{\partial g_{\theta\theta}}{\partial \theta}) u^\theta \right] (u_r u^\theta) \\ &\quad + \frac{\partial u_r}{\partial r} - \frac{1}{2} (g^{rr} \frac{\partial g_{rr}}{\partial r}) u^r \right] (u_r u^\theta) \\ &\quad \left. + \frac{\partial u_r}{\partial \theta} - \frac{1}{2} (g^{rr} \frac{\partial g_{rr}}{\partial \theta}) u^r \right] ((u^\theta)^2 + g^{\theta\theta}) \\ &\quad - \frac{2}{3} (\bar{\nabla}_r \cdot u^r + \bar{\nabla}_\theta \cdot u^\theta) (u_r u^r + 1) \right], \end{aligned} \quad (10)$$

$$\begin{aligned} L2_{r\theta}^\theta &= \bar{\nabla}_r \cdot \eta \left[\left(\frac{\partial u_\theta}{\partial r} - \frac{1}{2} (g^{\theta\theta} \frac{\partial g_{\theta\theta}}{\partial r}) u_\theta \right) (u^r)^2 + g^{rr} \right] \\ &\quad - \frac{2}{3} (\bar{\nabla}_r \cdot u^r + \bar{\nabla}_\theta \cdot u^\theta) (u_\theta u^r) \\ &\quad + \bar{\nabla}_\theta \cdot \eta \left[\left(\frac{\partial u^\theta}{\partial r} + \frac{1}{2} (g^{\theta\theta} \frac{\partial g_{\theta\theta}}{\partial \theta}) u^\theta \right) (u_\theta u^\theta + 1) \right. \\ &\quad \left. - \frac{2}{3} (\bar{\nabla}_r \cdot u^r + \bar{\nabla}_\theta \cdot u^\theta) (u_\theta u^\theta + 1) \right] \\ &\quad \left. + \left(\frac{\partial u^\theta}{\partial \theta} - \frac{1}{2} (g^{\theta\theta} \frac{\partial g_{\theta\theta}}{\partial \theta}) u^\theta \right) (u^\theta)^2 + g^{\theta\theta} \right], \end{aligned} \quad (11)$$

$$\begin{aligned} L2_{r\theta}^\varphi &= \bar{\nabla}_r \cdot \eta \left[\left(\frac{\partial u_\varphi}{\partial r} - \frac{1}{2} (g^{\varphi\varphi} \frac{\partial g_{\varphi\varphi}}{\partial r}) u_\varphi + g^{\varphi\varphi} \frac{\partial g_{\varphi\varphi}}{\partial r} \right) u_\varphi \right] (u^r)^2 + g^{rr} \\ &\quad + \left(\frac{\partial u_\varphi}{\partial \theta} - \frac{1}{2} (g^{\varphi\varphi} \frac{\partial g_{\varphi\varphi}}{\partial \theta}) u_\varphi + g^{\varphi\varphi} \frac{\partial g_{\varphi\varphi}}{\partial \theta} \right) u_\varphi \right] (u^r u^\theta) \\ &\quad - \left(\frac{1}{2} (g^{rr} \frac{\partial g_{rr}}{\partial r}) u^r u_\varphi u^t - \left(\frac{1}{2} (g^{rr} \frac{\partial g_{\varphi\varphi}}{\partial r}) u^\varphi (u_\varphi u^\varphi + 1) \right) \right. \\ &\quad \left. + \bar{\nabla}_\theta \cdot \eta \left[\left(\frac{\partial u_\varphi}{\partial r} - \frac{1}{2} (g^{\varphi\varphi} \frac{\partial g_{\varphi\varphi}}{\partial r}) u_\varphi + g^{\varphi\varphi} \frac{\partial g_{\varphi\varphi}}{\partial r} \right) (u^r u^\theta) \right. \right. \\ &\quad \left. \left. + \left(\frac{\partial u_\varphi}{\partial \theta} - \frac{1}{2} (g^{\varphi\varphi} \frac{\partial g_{\varphi\varphi}}{\partial \theta}) u_\varphi + g^{\varphi\varphi} \frac{\partial g_{\varphi\varphi}}{\partial \theta} \right) u_\varphi \right] ((u^\theta)^2 + g^{\theta\theta}) \right. \\ &\quad \left. - \left(\frac{1}{2} g^{\theta\theta} \frac{\partial g_{\varphi\varphi}}{\partial \theta} \right) u^\varphi u_\varphi u^t - \left(\frac{1}{2} g^{\theta\theta} \frac{\partial g_{\varphi\varphi}}{\partial \theta} \right) u^\varphi (u_\varphi u^\varphi + 1) \right], \end{aligned} \quad (12)$$

where $g_{\mu\nu}$ is the contravariant form of the metric tensor $g^{\mu\nu}$.

2.1. Simplifying considerations

Most of the above-described collection of viscous terms contains highly non-linear, first and second order operators, some of which are difficult to handle numerically or unnecessarily enlarge the band-width of the coefficient matrix, while others may

decelerate, rather than accelerate, the convergence of the numerical solution procedure. In 3D axi-symmetry, few of these terms can be simplified or even neglected without violating the physical consistency of the numerical scheme.

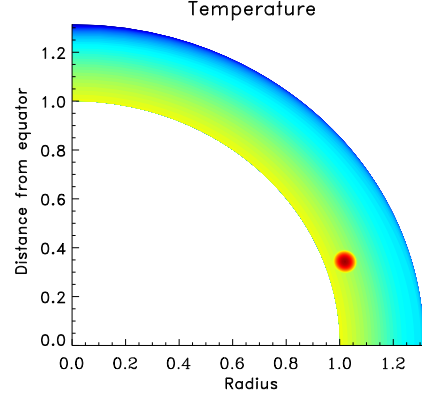


Fig. 1. The starting distribution of the temperature in the domain of calculation. Low (high) values correspond to blue (yellow) color. The red color corresponds to the hot bubble.

To outline our simplification strategy, we first mention the following relevant issues:

1. In most astrophysical fluid flows the molecular viscosity is too small to be relevant on observationally reasonable time scales. Thus, in the absence of other forms of viscosity, the above operators can be safely neglected. Moreover, these operators must vanish asymptotically whenever the fluid velocity approaches the speed of light.
2. Turbulent viscosity is more common in modeling astrophysical fluid dynamics. In rotating astrophysical flows, turbulent viscosity is a fundamentally important mechanism for angular momentum transport. Therefore, the viscous operators of the angular momentum equation are important and should converge to the usual Newtonian form whenever the velocity becomes sub-relativistic.
3. The viscous operators appearing in the radial and vertical momentum equations act, in general, to diffuse and smooth strong velocity-gradients. The mixed-derivative appearing in these two equations act to mainly enhance the viscous-coupling between the velocity components.

Therefore, our simplification strategy relies on considering only second order, mixed-free and Laplace-like operators. In numerical matrix algebra, such operators generally enhance the diagonal dominance of the coefficient matrix and stabilize its inversion procedure.

Specifically, using our time-implicit formulation, the following operators have been included into the numerical solver:

$$\begin{aligned} \tilde{L}2_{r\theta}^r &= \bar{\nabla}_r \cdot \{ \eta \left[2 \frac{\partial u^r}{\partial r} - \frac{2}{3} (\bar{\nabla}_r \cdot u^r) \right] \} (u_r u^r + 1) \\ &\quad + \bar{\nabla}_\theta \cdot \{ \eta \left(\frac{\partial u_r}{\partial \theta} \right) \} ((u^\theta)^2 + g^{\theta\theta}) \end{aligned} \quad (13)$$

$$\begin{aligned} \tilde{L}2_{r\theta}^\theta &= \bar{\nabla}_r \cdot \{ \eta \left[\left(\frac{\partial u_\theta}{\partial r} \right) (u^r)^2 + g^{rr} \right] \right. \\ &\quad \left. + \bar{\nabla}_\theta \cdot \{ \eta \left(\frac{\partial u^\theta}{\partial \theta} \right) - \frac{2}{3} \bar{\nabla}_\theta \cdot u^\theta \right] \} (u_\theta u^\theta + 1) + \left(\frac{\partial u^\theta}{\partial \theta} \right) (u^\theta)^2 + g^{\theta\theta} \} \end{aligned} \quad (14)$$

$$\begin{aligned} \tilde{L}2_{r\theta}^\varphi &= \bar{\nabla}_r \cdot \eta \left[\left(\frac{\partial u_\varphi}{\partial r} - \frac{1}{2} (g^{\varphi\varphi} \frac{\partial g_{\varphi\varphi}}{\partial r}) u_\varphi + g^{\varphi\varphi} \frac{\partial g_{\varphi\varphi}}{\partial r} \right) u_\varphi \right] (u^r)^2 + g^{rr} \\ &\quad - \left(\frac{1}{2} (g^{rr} \frac{\partial g_{\varphi\varphi}}{\partial r}) u^r u_\varphi u^t - \left(\frac{1}{2} (g^{rr} \frac{\partial g_{\varphi\varphi}}{\partial r}) u^\varphi (u_\varphi u^\varphi + 1) \right) \right. \\ &\quad \left. + \bar{\nabla}_\theta \cdot \eta \left[\left(\frac{\partial u_\varphi}{\partial r} - \frac{1}{2} (g^{\varphi\varphi} \frac{\partial g_{\varphi\varphi}}{\partial r}) u_\varphi + g^{\varphi\varphi} \frac{\partial g_{\varphi\varphi}}{\partial r} \right) (u^\theta)^2 + g^{\theta\theta} \right. \right. \\ &\quad \left. \left. - \left(\frac{1}{2} g^{\theta\theta} \frac{\partial g_{\varphi\varphi}}{\partial \theta} \right) u^\varphi u_\varphi u^t - \left(\frac{1}{2} g^{\theta\theta} \frac{\partial g_{\varphi\varphi}}{\partial \theta} \right) u^\varphi (u_\varphi u^\varphi + 1) \right] \right] \end{aligned} \quad (15)$$

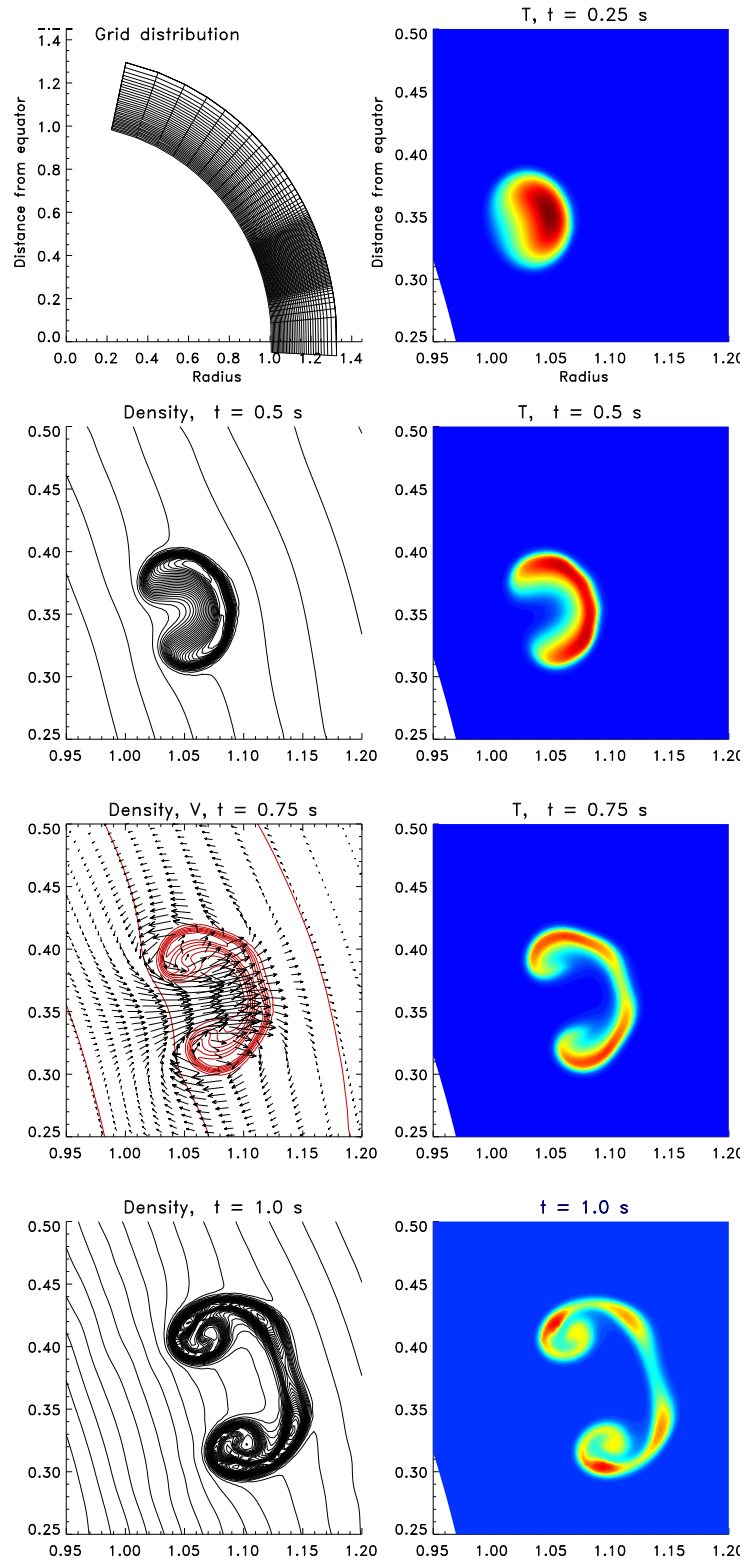


Fig. 2. a rising bubble in the white dwarf atmosphere. The domain of calculation is covered by 100×170 non-uniformly distributed finite volume cells (top left panel). The colored images are snapshots of the temperature of the rising bubble after 0.25, 0.5, 0.75 and 1.0 second after the flash. low-to-high values of temperature correspond to blue-to-red. On the left panel, snapshot of the density distribution at 0.5, 0.75 and 1.0 seconds in black-white are shown.

It can be easily verified that in the non-relativistic regime the radial component of the diffusion operator $\tilde{L}2_r^\varphi$ reduces to the classical Newtonian form:

$$\tilde{L}2_r^\varphi = \frac{1}{r^2} \frac{\partial}{\partial r} r^4 \eta \frac{\partial \Omega}{\partial r}, \quad (16)$$

where $\eta = \rho \nu$ and ν denotes the kinematic viscosity.

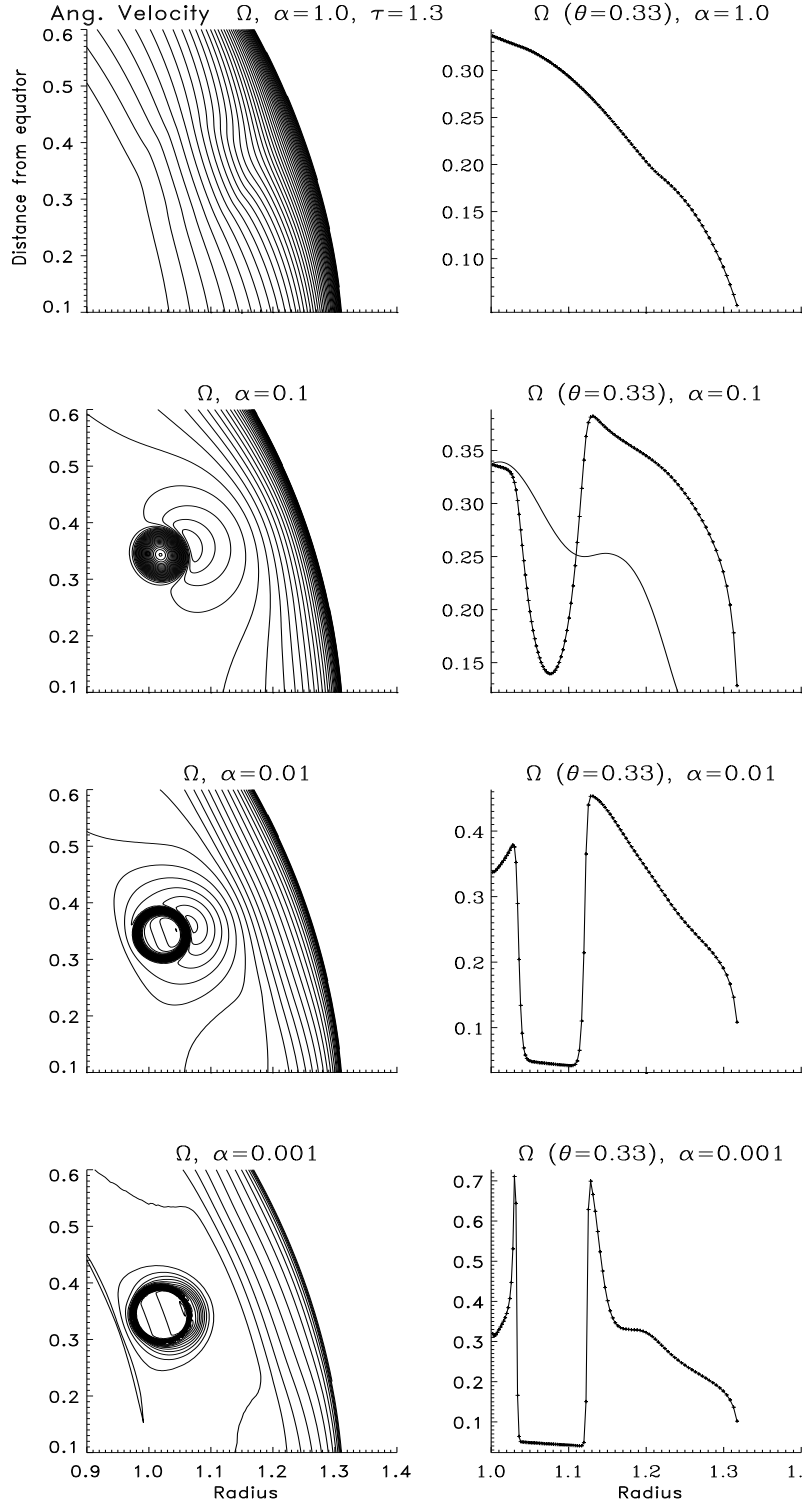


Fig. 3. The distribution of the angular velocity in the bursting region for four different viscosity parameters α_{tur} shortly after burst events ($\approx 0.1\text{ms}$). In the left panel 30 uniformly distributed isolines of the angular frequency Ω are shown. On the right panel we display the radial profiles of Ω across the bursting region. The solid line in “(b2) corresponds to a relaxed Ω -profile after 10 ms.

2.2. Viscosity prescription

Similar to classical accretion disks, we assume that molecular viscosity is too small to have a significant effect on the angular momentum distribution on a short time scale such as the thermonuclear one.

Therefore, we adopt the turbulent viscosity prescription:

$$\nu_{\text{tur}} \doteq \langle V_{\text{tur}} \rangle \langle \ell_{\text{tur}} \rangle \approx \alpha_{\text{tur}} V_S \times \alpha_2 R_{\text{NS}}, \quad (17)$$

where $\langle V_{\text{tur}} \rangle$, $\langle \ell_{\text{tur}} \rangle$ correspond to mean values of velocity and length scale of eddies in a turbulent medium, respectively.

These are set to be respectively smaller than the sound speed V_S and smaller than the radius of the NS. Thus, α_{tur} , α_2 are constants that are set to be smaller than unity. In the present paper, all model calculations assume $\langle \ell_{\text{tur}} \rangle = 0.1R_{\text{NS}}$, i.e., $\alpha_2 = 0.1$, whereas the parameter α_{tur} may differ from one model calculation to another.

3. Heat bubble calculations

3.1. Numerical solution method

The set of hydrodynamical equations are solved using a preconditioned defect-correction iteration procedure. The matrix equation to be solved in each iteration is:

$$\tilde{A}\mu = d, \quad (18)$$

where \tilde{A} is a preconditioner, i.e., a coefficient matrix that is similar to the Jacobian J , but which is much easier to invert. J is obtained by calculating the entries resulting from $\partial R/\partial q$, where R denotes the vector of equations (Eq. 4) and q the vector of variables.

In this formulation $\mu = q^{i+1} - q^i$ corresponds to the correction between two successive iterations and d is the defect (for a detailed description of the method see Hujeirat, 2005; Hujeirat et al., 2008).

We mention that the solver employed here relies on the conservative formulation of the hydrodynamical equations, using the finite volume formulation. For strongly time-dependent simulations, an advection scheme of third order spatial and second order temporal accuracies is used (Hujeirat, 2005). As pre-conditioner we use the approximate factorization method (AFM), which is proven to be most appropriate for modeling weakly and strongly low Mach number flows (Hujeirat et al., 2007).

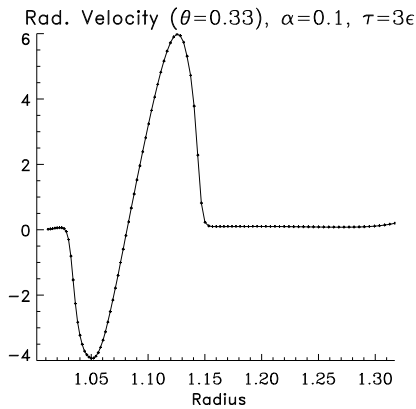


Fig. 4. The profile of the radial velocity across the heat bubble shortly after the burst (0.3 ms), using $\alpha_{\text{tur}} = 0.1$. Obviously, the outward-oriented fluid motion is much stronger than the inwards one.

3.2. Heat bubble propagation in the atmosphere of a non-rotating white dwarf

Rising bubbles in stellar environments have been extensively studied by Almgren et al. (2006, see also the references therein). To test the capability of our solver at capturing the propagation of strongly time-dependent heat bubbles in strong gravitational fields, such as X-ray bursts on neutron stars, we adopt the same

setup of the heat bubble problem as described in Sec. 4.3 of Almgren et al. (2006).

The domain of calculation is restricted to the first quadrant:

$$\begin{aligned} \mathcal{D} &= [R_{\text{in}} \leq r \leq R_{\text{out}}] \times [0 \leq \theta \leq \pi/2] \\ &= [1 \leq r \leq 1.35] \times [0 \leq \theta \leq \pi/2], \end{aligned}$$

where length scales are measured in units of the radius of the star's core.

The domain \mathcal{D} is divided into non-uniformly distributed finite volume cells: 100 in the radial and 170 in the horizontal direction, where the minimum grid spacings is set to coincide with the center of the initial heat bubble.

The initial conditions are constructed by carrying out 3D axisymmetric time-dependent calculation to obtain the hydrostatic equilibrium. A small region is then chosen (Fig. 1), where the matter is replaced by a thinner but much hotter plasma, while keeping it in pressure equilibrium with the surrounding media.

In Fig. 2 we show several snapshots of the rising bubble. Obviously, these results agree quite well with the unsplit and the low Mach number schemes presented by Almgren et al. (2006).

3.3. Rotating heat bubbles in deep gravitational fields of neutron stars

Similar to the Sec. (3.2), we apply our general relativistic solver to model the rise of a rotating bubble starting from below the atmosphere of a rotating neutron star. The radius of the neutron star's core R_{NS} is set to be equal to the following radius,

$$R_{\text{NS}} = 3 r_g (1 + \sqrt{1 - \Omega_{\text{NS}}^2}), \quad (19)$$

which is smaller than the classical last stable orbit of a Schwarzschild black hole. The inner boundary of the domain of calculation is taken to be the radius of the core, whereas the outer boundary is located at $R_{\text{out}} = 1.35R_{\text{NS}}$. The core is set to rotate at 0.4 the break-up velocity, whereas Ω at the outer radius is 10 times smaller. The matter in the domain is set to adjust its rotation to the boundaries through viscous interaction.

The initial distribution of the variables are obtained by solving the general relativistic Navier-Stokes equations to obtain stationary and differentially rotating flow configurations. As in the previous section, the heat bubble is injected into the domain through replacing the medium at a certain location by a hot and tenuous plasma, while keeping it in pressure and rotational equilibrium with the surrounding media.

Unlike the calculations in the previous section, the purpose of the present calculations is to unveil the response of the surrounding region to violent events associated with a dramatic change in the distribution of the angular momentum.

Therefore we run several numerical calculations with $\alpha_{\text{tur}} = 1.0, 0.1, 0.01, 0.001$. The initial stationary configurations have been obtained using the corresponding value of α_{tur} . The results are shown in Fig. 3 and can be summarized as follows:

1. All model calculations show a pronounced deficiency of angular momentum at the central part of the burst, accompanied with a significant increase at the boundary of the bubble. Thus, the burst leads to the formation of a dynamically unstable flow-configuration: a shell of slow rotating matter is bounded both from below and from above by relatively fast rotating matter.

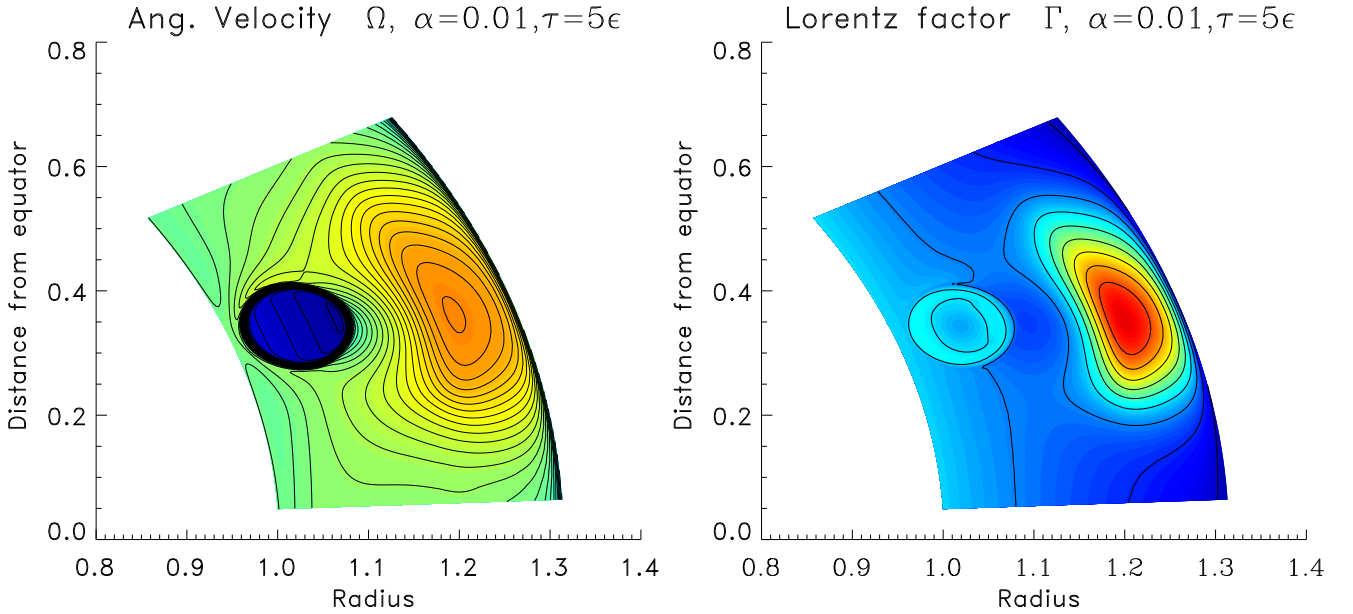


Fig. 5. 25 isolines of the angular velocity (left) and of the Lorentz factor (right panel) overlaid on their corresponding colored images after 0.5 ms are shown, using $\alpha_{\text{tur}} = 0.01$. Blue-to-red color correspond to low-to-high values of Ω and Γ .

2. The viscous-induced fronts of angular momentum are found to propagate outwards at much faster speed than inwards. This implies that the matter in the deeper layers adapts its conditions to the inner boundary much faster than at the outer boundary. This is a consequence of the adopted prescription of the viscosity η , which is more effective in hotter and denser regions of the plasma. Also, the outwards-oriented velocity is obviously larger than the inward one (Fig. 4).
3. The difference between the rotational velocity at the center of the bubble and that at its boundaries becomes more significant, the smaller the α_{tur} -parameter is chosen.

In the $\alpha_{\text{tur}} = 1.0$ case (see Fig. 3 (a1)), the rise time of the bubble is found to be extremely long compared to those obtained with smaller α_{tur} .

Here the viscous pressure in the radial direction $P_{\text{visc}}^r \sim \alpha_{\text{tur}} \frac{\partial u}{\partial r}$ has an opposite sign and acts to reduce the effects of the thermal pressure P_{th} . In the extreme case, when $P_{\text{th}} + P_{\text{visc}} \rightarrow 0$, the effective sound speed, $V_S^{\text{eff}} \sim \delta(P_{\text{th}} + P_{\text{visc}})/\delta\rho \rightarrow 0$, hence the propagation time $\tau_{\text{pro}} \sim R/V_S^{\text{eff}} \rightarrow \infty$.

On the other hand, τ_{pro} becomes of the order of one second, when using $\alpha_{\text{tur}} \sim \mathcal{O}(10^{-1})$, which fits well into the observed duration of burst events on NSs.

In the low α_{tur} cases, (see Fig. 3 b1,c1,d1 and Fig. 5), the significant increase of the rotational velocity at the outer Ω -fronts is obvious, but unreasonably large. In the Fig. 2 (d1), the matter at the outer front is found to be gravitationally unbound to the central NS, giving rise to strong outflows.

However, as outflows during X-ray bursts can be excluded on observational grounds, we conclude that α_{tur} must acquire much larger values, and that specifically $\alpha_{\text{tur}} \sim \mathcal{O}(10^{-1})$.

To study the viscous-reaction of the matter in the adjusting layers to the sudden increase of rotation induced by a burst, we have run separate calculations in the following manner. A solution for the hydrodynamical equations including rotation has been hydrodynamically calculated. As a second step, we modified the Ω -profile by including a Gaussian perturbation of the form depicted in Fig. 6/ τ_0 . We then followed the time evolution of this

profile on the viscous time scale. The profiles $\tau_1, \tau_2, \tau_{10}$ correspond to $\tau_{\text{visc}}/10, \tau_{\text{visc}}/5, \tau_{\text{visc}}$.

These calculations show that the effect of turbulent viscosity is to mainly transport angular momentum outwards. As a consequence, the deficiency in the rotational support in the deep layers enhances the compression of matter and give rise to an additional burst in the neighboring shell. This chain of reactions may run away to spread over the whole surface of the NS on the viscous time scale, which is of the order of one second, assuming $\alpha_{\text{tur}} \approx 0.1$.

When the outer layers cool, the turbulent viscosity decreases and the corresponding viscous time scale increases as $\tau_{\text{visc}} \sim 1/\sqrt{T}$. This implies that after the burst, the time scale needed for the outer layers to adjust their rotation to the bulk of the star might lengthen by an additional order of magnitude. As a consequence, the observed spin up of NSs in their cooling tail is a manifestation of the increased rotational velocity of the outer layers caused by the burst events, but which, eventually, should decrease at later times.

4. Summary & Conclusions

In this paper we have presented the set of general relativistic Navier-Stokes equations in 3D axi-symmetry, using the Boyer-Lindquist coordinates in the background of a slowly rotating neutron star. We have shown that, for modeling relativistic viscous flows, the collection of viscous operators can be reduced considerably into a smaller class, which consists of the dominant second order operators, and which subsequently enhances convergence of the implicit solution procedure.

The set of equations are solved numerically using an implicit solution procedure, which is based on a pre-conditioned defect-correction iterative method. Similar to Taylor-flows between concentric spheres, we use the "Approximate Factorization Method" as a pre-conditioner, which has superior converging properties over other non-symmetric methods, such as the black-white line Gauss-Seidel method. In the non-rotating case, we have shown that the solver is capable of reproducing the time-evolution of heat bubbles during their rise to the surface of

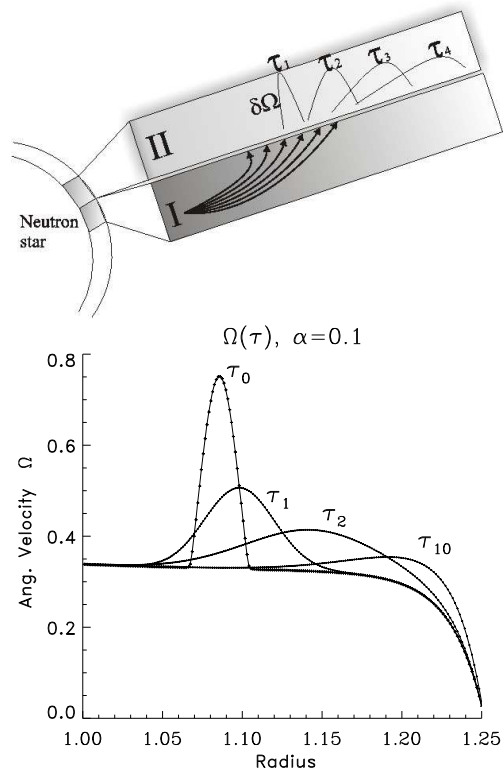


Fig. 6. Successive snapshots of the omega-profiles in the outer layers of a neutron star. Shell I shows the burst-induced propagation of Omega-fronts into the neighboring shells. In shell II, the viscous-induced reaction to the Omega-fronts is shown. This schematic picture shows that viscosity transport the excess of angular momentum preferably in the outward direction. The lower figure, which is obtained using hydrodynamical calculations, clearly confirms this behavior.

the white dwarfs, as reported by Almgren et al. (2006); Nonaka (2008), accurately.

In the rotating case, it has been shown that viscous-generated fronts inside heat bubbles propagate into the surrounding quite rapidly. The effect of these front is mainly to transport angular momentum to the outer layers, leaving the matter in the deeper layer with less rotational support, hence more compressed.

The increased rotational velocity of the outer layers may be connected to the observed spin up of neutron stars during X-ray bursts. However, this increase will eventually be followed by a spin down on later times when the outer layers cooled down to their pre-burst thermal state.

Our numerical results show that a viscosity parameter of the order of $\alpha_{\text{tur}} \sim 0.1$ is the most suitable value for fitting observations of NSs during X-ray bursts. A much larger value yields propagational time that is much larger than one second, whereas smaller values yield unstable shell configurations and gives rise to gravitationally unbound outflows.

In addition, a possible mechanism that may underly the rapid spreading of burning ignition fronts has been presented. Accordingly, the viscous-generated fronts inside a heat bubble may transport angular momentum into the horizontally adjusting layers. The viscosity then acts to decouple matter from angular momentum, subsequently enhancing compression in the deeper layers and giving rise to thermonuclear runaway. This chain of reactions may run away to spread over the whole surface of the NSs on the viscous time scale $\tau_{\text{vis}} \sim 1$ s.

Concerning frame dragging, while included in the present simulations, its effects are still to be quantified. Also, the effects of

magnetic fields and thermal diffusion is the subject of an ongoing work.

Acknowledgment AH thanks Max Camenzind for the the valuable discussions and Bernhard Keil and Paul P. Hilscher for carefully reading the manuscript. This work is supported by the Klaus-Tschira Stiftung under the project number 00.099.2006.

References

- Abdikamalov, E.B., Dimmelmeier, H.; Rezzolla, L.; Miller, J.C., 2008, *Astro-ph/080617*
- Almgren, A.S., Bell, J.B., Rendleman C.A. and M. Zingale, 2006, *ApJ*, 649, 927
- Baiotti, L., Hawke, I., Montero, P.J., et al., 2005, *PhRvD*, 71, 4035
- Bildsten, L., Strohmayer, T., *Phys. Today*, 52, 2, 40
- Camenzind, M., 2007, “Compact Objects in Astrophysics”, Springer-Verlag GmbH
- Cumming, A., Bildsten, L., 2000, *ApJ*, 544, 453
- Duez, M.D., Liu, Y.T., Shapiro, S.L., et al., 2004, *PhRvD*, 69, 104030
- Font, J.A., 2003, *LRR*, 6, 4
- Hujeirat, 2005, *CoPhC*, 168
- Hujeirat, A., Thielemann, F.-K., Dusek, J., Nusser, A., 2007, *astro-ph/0712.3663*
- Hujeirat, A., Keil, B.W., Heitsch, F., 2007b, *astro-ph/0712.3674*
- Hujeirat, A., Camenzind, M., Keil, B.W., 2008, *NewA*, 13, 436
- Liebendörfer, M., Rosswog, S., Thielemann, F.-K., 2002, *ApJS*, 141, 229
- Marti, J.M., Müller, E., 2003, *LRR* 6
- McKinney, J.C., 2006, *MNRAS*, 368, 30
- Migliari, S., Fender, R.P., 2006, *MNRAS*, 366, 79
- Migliari, S., 2008, *AIPC*, 1010, 23
- Nonaka, A., Almgren, A., Bell, J., et al., 2008, *AAS*, 212, 1605
- Özel, F., Psaltis, D., 2003, *ApJ*, 582, 310
- Pringle, J.E., 1981, *ARA&A*, 19, 137
- Psaltis, D., 2006, in *Compact stellar X-ray sources*, Ed. Lewin, et al., CUP, 39, 1
- Psaltis, D., 2008, *PhRvD*, 77, 4006
- Richardson, G.A., Chung, T.J., 2002, *ApJSS*, 139, 539
- Shibata, M., Liu, Y.T., Shapiro, S.L., Stephens, B.C., 2006, *PhRvD*, 74, 4026
- Shibata, M., 2003, *ApJ*, 595, 992
- Shapiro, S.L., Saul A. Teukolsky, S.A., 1983, “Black Holes, White Dwarfs and Neutron Stars”, John Wiley & Sons Inc
- Spitkovsky, A., Levin, Y., Ushomirsky, G., 2002, *ApJ*, 566
- Stergiouas, N., 2003, *Livingreviews*, LRR-2003-3
- Strohmayer, T.E., Zhang, W., Swank, J.H., 1997, *ApJ*, 487, 77
- Strohmayer, T.E., 2001, *AIPC*, 599, 377
- Strohmayer, T.E., 2001b, *AdSpR*, 28, 511
- Strohmayer, T.E., Markwardt, C.B., 1999, *ApJ*, 516, 81
- Strohmayer, T.E., 1999, *AAS*, 194, 2901
- Strohmayer, T.E., 1999, *ApJ*, 523, 51
- Thielemann, F.-K., Hashimoto, M.-A., Nomoto, K., 1990, *ApJ*, 349, 222
- Etienne, Z.B., Faber, J.A., Liu, Y.T., Shapiro, S.L., et al, 2008, *PhRvD*, 77, 4002,
- Zingale, M., Almgren, A.S., Bell, J.B., et al., 2006, *JPhCS*, 46, 385